Nonlinear Dynamic Modeling of Isometric Force Production in Primate Eye Muscle

Sean R. Anderson*, Nathan F. Lepora, John Porrill, and Paul Dean

***Abstract*—Although the oculomotor plant is usually modeled as a linear system, recent studies of ocular motoneuron behavior have drawn attention to the presence of significant nonlinearities. One source of these is the development of muscle force in response to changes in motoneuron firing rate. Here, we attempt to simulate the production of isometric force by the primate lateral rectus muscle in response to electrical stimulation [A. Fuchs and E. Luschei, "Development of isometric tension in simian extraocular muscle," *J. Physiol.*, vol. 219, no. 1, pp. 155–166, 1971] by comparing four different modeling approaches. The data could be well fitted either by parameter estimation for physically based models of force production [J. Bobet, E. R. Gossen, and R. B. Stein, "A comparison of models of force production during stimulated isometric ankle dorsiflexion in humans," *IEEE Trans. Neural Syst. Rehabil. Eng.*, vol. 13, no. 4, pp. 444–451, Dec. 2005; E. Mavritsaki, N. Lepora, J. Porrill, C. H. Yeo, and P. Dean, "Response linearity determined by recruitment strategy in detailed model of nictitating membrane control," *Biol. Cybern.*, vol. 96, no. 1, pp. 39–57, 2007], or by the application of a generic method for nonlinear system identification (the nonlinear autoregressive with exogenous input (NARX) model). These results suggest that nonlinear system identification may be a useful method for modeling more general aspects of muscle function, and provide a basis for distributed models of motor units in extraocular muscle for understanding dynamic oculomotor control. The success of previous linear models points to the potential importance of motor unit recruitment in overcoming nonlinearities in the oculomotor plant.**

***Index Terms*—Lateral rectus, muscle, nonlinear, nonlinear autoregressive with exogenous input (NARX), oculomotor plant, system identification.**

I. Introduction

EYE-MOVEMENT control has been studied both for its own sake, and as a potential guide to the general principles underlying biological motor control [1]. Since one of the major generic problems facing neural controllers is how to deal with the nonlinearities inherent in biological tissue (e.g., [2]), it is natural to ask how this problem is addressed in the oculomotor system.

Manuscript received September 1, 2009; revised January 20, 2010; accepted February 17, 2010. Date of publication May 3, 2010; date of current version June 16, 2010. This work was supported by the Novel Computation Initiative, Engineering, Physical Sciences Research Council (EPSRC), U.K. under Grant GR/T10602/01. *Asterisk indicates corresponding author.*

*S. R. Anderson is with the Centre for Signal Processing in Neuroimaging and Systems Neuroscience and Department of Psychology, University of Sheffield, Sheffield, S102TP, U.K. (e-mail: s.anderson@sheffield.ac.uk).

N. F. Lepora, J. Porrill, and P. Dean are with the Centre for Signal Processing in Neuroimaging and Systems Neuroscience and Department of Psychology, University of Sheffield, S10 2TP Sheffield, U.K. (e-mail: n.lepora@sheffield.ac.uk; j.porrill@sheffield.ac.uk; p.dean@sheffield.ac.uk).

Digital Object Identifier 10.1109/TBME.2010.2044574

Although in the past, there has been an emphasis on the linear aspects of oculomotor control (e.g., [3]), more recent investigations have begun to focus on the potential importance of nonlinearities in the oculomotor plant. Sylvestre and Cullen recorded from neurons in the primate abducens nucleus during both fast and slow eye movements [4]. They found that, for horizontal movements in the pulling direction of the lateral rectus muscle innervated by the abducens nucleus, neuronal firing rates could be related to eye-movement kinematics by a second-order linear equation, provided the velocity range was restricted. However, when the full range of eye-movement velocity (∼20°/s–400°/s) was considered, the equation coefficients varied significantly [4, Fig. 14].

The production of eye movements by changes in motoneuron firing rates involves a cascade of dynamic processes (see Fig. 1). Analysis of the eye-movements produced by microstimulation of the abducens nucleus in alert primates [5] drew attention to one of these processes, the production of isometric force by the lateral rectus muscle, as a potential source of nonlinearity. Fuchs and Luschei [6] had previously shown that stimulation of the isolated muscle produced a steady-state muscle force that was a sigmoidal function of stimulation frequency, and that at stimulation onset muscle force rose more rapidly the higher the frequency [see Fig. 2(f)]. Very similar nonlinearities were observed for stimulation-produced eye displacement [5]. In contrast, analysis of the return movements of the eye after stimulation offset indicated that the mechanics of the oculomotor plant were approximately linear for the range of eye displacements investigated, in accord with previous analyses [7]–[10]. These results suggest that the conversion of motoneuron firing into isometric force is a potentially important source of nonlinearity of oculomotor control.

The nonlinearities described by Fuchs and Luschei [6] for the primate lateral rectus muscle have been observed for other extraocular rotatory muscles in a variety of species [11]–[16] and appear to be characteristic of skeletal muscle in general [17]–[19]. It is perhaps surprising then that they have not hitherto been specifically addressed in models of the oculomotor plant [5], [20], [21]. The purpose of the present study was, therefore, to model the nonlinearities described by Fuchs and Luschei [6], for inclusion in future models of oculomotor control. Since there are a number of different methods available for modeling nonlinearities, we compared the following plausible candidate methods.

1) A simplification that has been found useful for biological problems is to combine linear dynamics with static nonlinearities [2]. Often a low parameter description of the static nonlinearity is feasible, so, overall identification is only

slightly more complex than with linear models. Here, we chose the Wiener architecture, in which the nonlinearity comes after the linear dynamics and a related structure—a parallel cascade of Wiener models [22]. A possible alternative, the Hammerstein arrangement, in which the nonlinearity comes before the dynamics reduces to the general linear model for the stimulation conditions used here (cf., [23]).

2) Physically based modeling can identify nonlinear dynamics from consideration of the underlying physics and chemistry of the system, for example, calcium dynamics in the case of muscle modeling (e.g., [23], [24]). These can be models with a small number of parameters, some of which may be known *a priori*. Here, we examined three physically based models. The first, the virtual muscle model [25] has a number of components that describe, e.g., length and velocity effects—here, we examined its performance in the isometric case. The second has been used to describe the nonlinear dynamics of the rabbit retractor bulbi muscle in producing conditioned eyeblink responses of the nictitating membrane [24], [26]–[28]. The retractor bulbi muscle is an extraocular muscle similar in a number of respects to the extraocular muscles that rotate the eye, so, this model is particularly relevant to the present study. Third, we used the Bobet and Stein model [23], on the basis of its successful performance in simulating isometric force production by human ankle dorsiflexors in comparison with six other models.
3) More general methods for nonlinear system identification that are based on series expansion of the output into products of the input at various lags (e.g., Volterra and Wiener series) require large numbers of parameters to describe even relatively simple systems [29]. However, nonlinear dynamic models that use basis function expansions of inputs *and* outputs such as the nonlinear autoregressive with exogenous inputs (NARX) model, typically require far fewer parameters [30]. They also allow systematic methods for choosing model structure, and can be implemented simply in a computationally efficient manner. We, therefore, chose a nonlinear input-output model as our third method of identifying nonlinearities in force production by oculomotor muscle.

The use of these different approaches provided an opportunity for comparison and benchmarking. For further comparison we also applied linear modeling techniques [31], to assess the advantage in using the more complex nonlinear descriptors.

The paper is organized as follows: The details of the experimental data used for modeling and the methodology explaining the model fitting for the linear and nonlinear models are given in Section II. The results of model fitting to the force profiles are given in Section III. The results of modeling the force profiles are discussed in Section IV.

II. Methods

A. Overview

The objectives of this investigation were to identify and compare linear and nonlinear models of lateral rectus dynamics in primate, that is, the transformation of the stimulation signal (pulse inputs u_t) to isometric force (y_t) as illustrated in Fig. 1. The identification methods were based on linear, Wiener, parallel cascade, virtual muscle model, Bobet and Stein, Bartha and Thompson, and nonlinear input–output models, applied to data extracted from Fuchs and Luschei [6], hereafter, referred to as FL71. The data extraction and modeling methods are described in the subsequent sections.

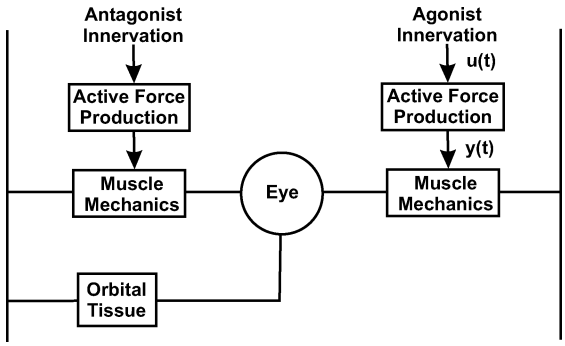

Fig. 1. Simplified diagram of oculomotor plant for horizontal eye movements. Horizontal eye movements are primarily controlled by a pair of muscles (medial and lateral rectus), whose net force acts on the plant mechanics (muscles plus orbital tissue) to alter eye position and velocity. In the simplified treatment used here, the relation between control signal (agonist and antagonist innervation) and eye movement consists of two dynamic processes. The first corresponds to the transformation of changes in innervation (increase in agonist, decrease in antagonist) into changes in active force. Here, we only examine isometric force but in the case of natural movements the active force would also be a nonlinear function of length and velocity. The second process corresponds to the transformation of changes in net force into movements of the eye.

B. Data

The signals used for modeling in our study were extracted from a historical dataset: recordings of isometric force produced by artificial stimulation of the lateral rectus in primate by FL71 (see [6] for details).

The force signals were obtained from a scanned version of Fig. 3(a) from FL71. A digital plotting software tool was used to extract the signals, *Plot Digitizer*,[1] where the force signals were discretely (and irregularly) sampled by point-and-click. The extraction software was accurate to the extent that all collected samples were within the plotted width of the force curve lines. The irregularly sampled force signals were interpolated by a spline function in MATLAB and resampled at 500 Hz to provide regular samples (using the MATLAB function *resample*). The force signals were then smoothed by the application of a second-order Butterworth filter (cutoff frequency 125 Hz). To avoid effects of phase shift, the signals were filtered in both a forward and backward direction.

The stimulation frequencies of the input signals were 100, 200, 300, 400, and 500 Hz, respectively. The durations of stimulation were specified in FL71 as between 100 and 150 ms; the number of pulses in each spike train were not specified, hence, these were estimated here from the force response curves. For the 100 Hz stimulation frequency, the number of pulses was obtained by examining the force curve directly, where the number

[1] http://plotdigitizer.sourceforge.net/.

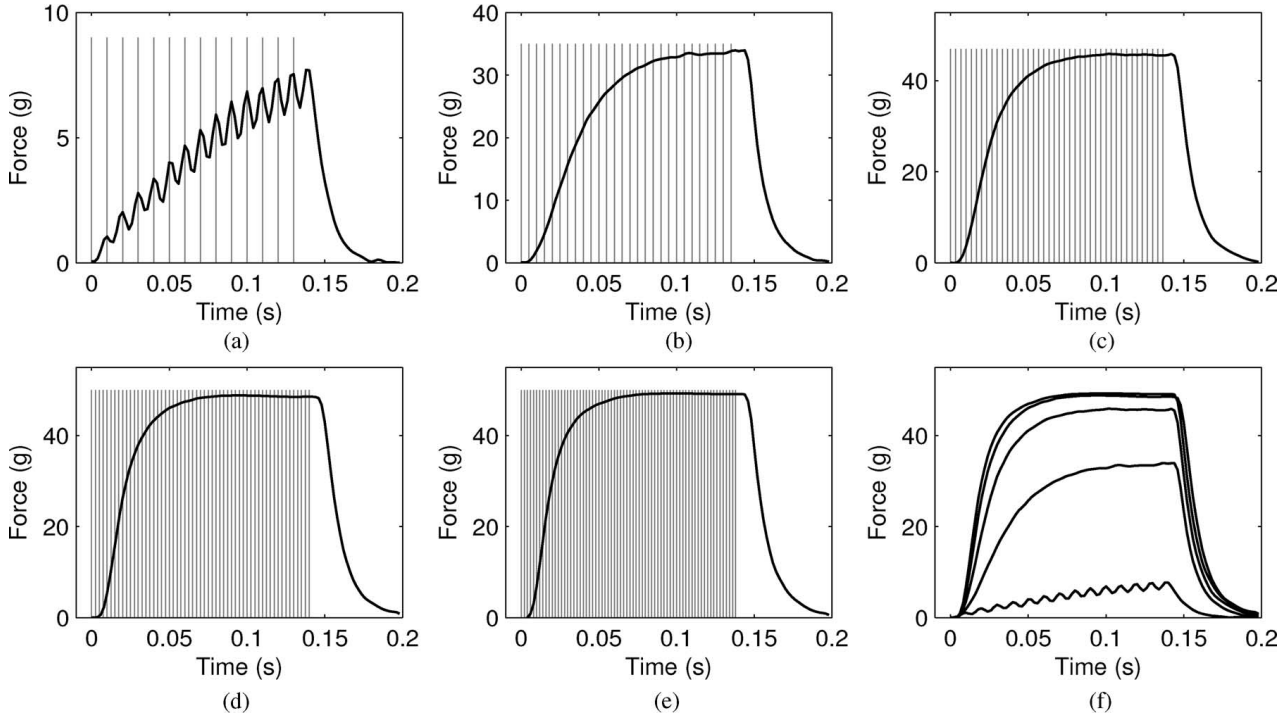

Fig. 2. Input–output modeling data extracted from Fuchs and Luschei [6]. Isometric force curves are shown in black and pulse trains are illustrated in gray. (a) 100 Hz, (b) 200 Hz, (c) 300 Hz, (d) 400 Hz, and (e) 500 Hz, (f) Combined force profiles 100–500 Hz.

of pulses (14) were clearly evident from the visible twitches in the force recording. For the other stimulation frequencies, the following method was used: the duration of a pulse train was defined between the times of the first and final pulses, T_0 and T_1, respectively. The time of the first pulse T_0 was defined as zero for each stimulation frequency. The time of the final pulse T_1 was defined relative to the onset of decay in the force recording T_2, i.e., $T_1 = T_2 - T_P$, where $T_P = 7$ ms was the twitch response time from a pulse to peak muscle force reported in FL71. The decay onset times T_2 were estimated by visual inspection of the force curves. The number of pulses was, therefore, estimated to be 14, 28, 42, 57, and 70, corresponding to the frequencies of stimulation 100–500 Hz.

Each pulse was constructed as a Dirac delta function (i.e., the magnitude of the pulse was equal to the sample frequency of the pulse train) as in [23]. The pulse trains were constructed at a frequency of 2.4 kHz (except the 500 Hz train, which was constructed at 2.5 kHz so that pulses occurred at evenly spaced sample times). For use in the identification procedures the pulse trains were resampled to 500 Hz to correspond to the force signals. The force signals extracted from FL71 are shown in Fig. 2 along with a scaled illustration of each pulse train.

C. Linear Modeling of Force Production

A single-input single-output linear time-invariant system can be represented in discrete-time by the model description [31]

$$y_t = G(q, \boldsymbol{\theta}) u_{t-d} \tag{1}$$

where in this case $y_t \in \mathbb{R}$ is the system output (isometric muscle force) at sample time t, $u_t \in \mathbb{R}$ is the system input (pulse train), d is a time delay in samples and the muscle dynamics are represented by the linear filter

$$G(q, \boldsymbol{\theta}) = \frac{b_1 q^{-1} + \cdots + b_{n_b} q^{-n_b}}{1 + a_1 q^{-1} + \cdots + a_{n_a} q^{-n_a}} \tag{2}$$

where q is the forward shift operator, i.e., $q y_t = y_{t+1}$ and the parameter vector $\boldsymbol{\theta} = (a_1, \ldots, a_{n_a}, b_1, \ldots, b_{n_b})$.

In addition to the input dynamics $G(q, \boldsymbol{\theta})$ in (1), it is common to include a noise model to further describe the system, which then determines the categorization of the model as autoregressive with exogenous inputs (ARX), output error (OE), or a number of other types [31]. We considered process noise to be negligible in this dataset and measurement noise to be more significant (due to the method used for extracting the signals), hence, we used the OE model structure and estimated the parameters using a prediction error method [31]. The parameter estimation cost function was the sum-of-squared (simulated prediction) error (SSE), i.e., $J = \sum_{t=1}^{N} (y_t - \hat{y}_t)^2$, where $\hat{y}_t$ was the simulated model output and N was the number of data samples. The algorithm used to estimate the parameters was the Nelder–Mead simplex method (implemented in MATLAB by the *fminsearch* function). Parameter estimates were initialized by least squares [32].

Previous investigations into linear modeling of oculomotor muscle force have determined that the 2 pole 1 zero structure is a good descriptor [33], [34]. A single linear model was identified in both a batch mode using all signals, which gave poor results (as expected). Hence, in order to further clarify the ability of a linear model to fit the force curves, linear models were used to fit each force curve separately. In order to check whether a

more complex model could improve the description, we fitted a finite impulse response (FIR) model to the data (i.e., by setting $n_a = 0$ in $G(q, \boldsymbol{\theta})$).

Time-delay was included in the model by visual inspection of the force curves. Due to the fact that the force was zero at the onset of stimulation, the time-delay in the response was simple and accurate to fix manually and had the advantage of removing a parameter from the structure-detection procedure. The time-delay d was established to be $d = 2$ samples, equivalent to 4 ms and was applied to all models discussed here (linear and nonlinear, respectively).

All models of isometric force profiles obtained here were validated by comparison of the model simulation with the recorded signals. In the case of this investigation, separate validation data were not available to allow a cross-validation procedure, hence, the fitting data was used in validation. Variance estimates for the model parameters were obtained by using the resampling of residual error approach [35].

D. Wiener Modeling and Cascaded Wiener Modeling of Force Production

The Wiener model is a representation of a nonlinear system, where the dynamics are described by a linear model and there is a static nonlinearity at the model output [2], [31]. It is an attractive representation for a nonlinear system because it is a simple extension of the linear model described earlier in (1); the Wiener model is

$$z_t = H(q, \boldsymbol{\zeta}) u_{t-d} \tag{3}$$

$$y_t = f\left[z_t\right] \tag{4}$$

where $f(.)$ is some nonlinear function describing the static nonlinearity at the output of the dynamic linear model, and $H(q, \boldsymbol{\zeta})$ is a linear dynamic model defined analogously to $G(q, \boldsymbol{\theta})$

$$H(q, \boldsymbol{\zeta}) = \frac{g_1 q^{-1} + \cdots + g_{n_g} q^{-n_g}}{1 + f_1 q^{-1} + \cdots + f_{n_f} q^{-n_f}} \tag{5}$$

where $\boldsymbol{\zeta} = \left(f_1, \ldots f_{n_f}, g_1, \ldots g_{n_g}\right)$.

The nonlinearity in the Wiener model is typically unknown and can be specified as, e.g., a polynomial. In our case, we had useful data to inform us about a possible structure: the force data was in the form of constant inputs at increasing stimulation frequencies. Therefore, we could visually observe that there was a sigmoidal saturation in the output (from a plot of peak input versus peak output—see Section III, Fig. 3). The specific sigmoidal function we used to represent the nonlinearity was

$$f_{\text{sig}}\left[z_t\right] = \frac{k_1}{1 + k_2 e^{-k_3 (z_t + k_4)}} - k_5. \tag{6}$$

All parameters of the Wiener model, $(\boldsymbol{\zeta}, k_1, \ldots, k_5)$, were estimated in an output error framework similarly to the linear modeling methods described earlier. The output error minimization was initialized by first fitting the static nonlinearity sigmoidal parameters, using normalized stimulation frequency as input and the corresponding peak force values as output. The linear dynamic part of the model $H(q, \boldsymbol{\zeta})$ was then initialized by transforming the force values through the inverse of the (initialized) sigmoidal function to give an estimate of the linear output $\hat{z}_t$. The initial parameters of $H(q, \boldsymbol{\zeta})$ were then estimated using least squares from the input–output pairs $(u_t, \hat{z}_t)$.

The Wiener model can be extended by a parallel cascade of Wiener models [22]. This is where a number of Wiener models are arranged in parallel, excited by the same input and the output obtained from summation across each model output, so that

$$y_t = \sum_{i=1}^{n_c} f_i \left[H_i(q, \boldsymbol{\zeta}_i) u_{t-d}\right] \tag{7}$$

where n_c is the number of cascades. The fitting procedure proposed by Korenberg [22] was used here: we fitted a Wiener model to the input–output data, and then a subsequent Wiener model to the residual error, and so on until the desired accuracy was reached. We used a high-order FIR model to describe the linear dynamics and a polynomial function as the static nonlinearity. Parameters were estimated by the Nelder–Mead simplex method (implemented in MATLAB by the *fminsearch* function) and were initialized by least squares.

E. Virtual Muscle (VM) Model

The VM model [25] incorporates many features of muscle behavior including force–length and force–velocity relationships. The study on force activation dynamics [17] is of particular relevance here. In order to investigate the VM model, we used the activation function from the model relevant to isometric recordings from artificial stimulation (i.e., ignoring effects of length, velocity, yield, and recruitment). In addition, sag was not observed in the FL71 data, and therefore, was also ignored for these purposes.

The activation dynamics model is based on first converting the spike train to a frequency envelope, by convolving the spike train with a smoothing function. In our case, this was equivalent to the low-pass filter applied to the spike train after resampling (described earlier). The model uses/produces normalized inputs f_{env} and outputs Af, hence, the normalized input u was defined as f_{env} and normalized output y as Af. The input f_{env} was filtered through a second-order dynamic function, defined in [17] as two first-order equations

$$\dot{f}_{\text{int}}(t, f_{\text{env}}, L) = T_f^{-1} \left[f_{\text{env}}(t) - f_{\text{int}}(t)\right] \tag{8}$$

$$\dot{f}_{\text{eff}}(t, f_{\text{int}}, L) = T_f^{-1} \left[f_{\text{int}}(t) - f_{\text{eff}}(t)\right] \tag{9}$$

where

$$T_f = \begin{cases} T_{f1} L^2 + T_{f2} f_{\text{env}}(t), & \dot{f}_{\text{eff}}(t) \geq 0 \\ L^{-1}(T_{f3} + T_{f4} Af), & \dot{f}_{\text{eff}}(t) < 0. \end{cases} \tag{10}$$

The length parameter L in this case was set to unity. The dynamic output f_{eff} was filtered through a static activation function, defined from [17] as

$$Af(f_{\text{eff}}) = 1 - \exp\left[-\left(\frac{f_{\text{eff}}}{a_f n_f}\right)^{n_f}\right]. \tag{11}$$

Parameters of the model $(T_{f1}, T_{f2}, T_{f3}, T_{f4}, a_f, \text{and } n_f)$ were estimated by the Nelder–Mead simplex method (implemented

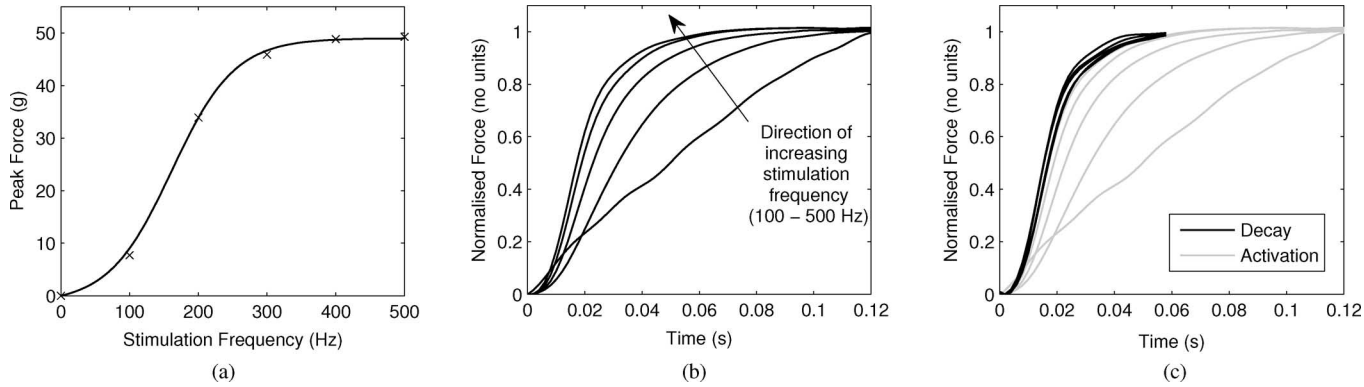

Fig. 3. Nonlinear features in the lateral rectus isometric force profiles. (a) Saturation in force profiles modeled by a sigmoidal function. (b) Normalized force activation dynamics, showing increasing rate of response with stimulation frequency. (c) Comparison of normalized force decay and activation dynamics (where the decay curves are reversed in sign and aligned on the time axis for an effective visual comparison with activation).

in MATLAB by the *fminsearch* function) and parameters were initialized from the values in [17].

F. Bobet and Stein Modeling of Force Production

The Bobet and Stein model of force production [36] is a sequence of a linear transfer function, a static nonlinearity and a time-varying linear transfer function. The equations for the Bobet and Stein model used here are the discrete versions, which are given in [23]; the input first-order linear filter represents calcium dynamics (note that where possible the original notation is kept)

$$c_t = Tu_{t-d} + a_1 c_{t-1} \tag{12}$$

where c_t is the calcium transient at sample time t, T is the sample time and we have explicitly introduced the sample delay d into the Bobet and Stein model description. The static nonlinearity represents the number of available cross-bridge sites

$$q_t = \frac{c_t^n}{c_t^n + k_0^n} \tag{13}$$

where k_0 and n are muscle-specific constants. The output time-varying first-order linear filter gives the proportion of attached cross-bridges

$$f_t = Tb_t^{(1)} q_t + b_t^{(2)} f_{t-1}. \tag{14}$$

We note that there are typographical errors in the specification of (14) in [23] that are corrected here using the original continuous-time model specified in [36]. The gain and time constant of the output filter are time-varying and the relevant parameters $b_t^{(1)}$ and $b_t^{(2)}$ are given by

$$b_t^{(1)} = b_0 \left(1 - \frac{b_1 f_{t-1}}{B}\right)^2 \tag{15}$$

$$b_t^{(2)} = e^{-b_t^{(1)} T} \tag{16}$$

where the parameter b_1 was constrained to lie in the range (0,1), as specified in [36]. Finally, the output is scaled by a gain parameter B, so that muscle force is given by

$$y_t = Bf_t. \tag{17}$$

The model comprised six parameters in total $(a_1, n, k_0, b_0, b_1,$ and $B)$. The parameters were estimated using the Nelder–Mead simplex method (implemented in MATLAB by the *fminsearch* function). As in [23] the parameters were initialized by hand. To implicitly constrain the range of the parameter b_1, the actual parameter obtained in the estimation procedure was $\bar{b}_1$, which is

$$b_1 = \frac{1}{e^{-\bar{b}_1} + 1} \tag{18}$$

where $\bar{b}_1 \in (-\infty, \infty)$, which ensured that $b_1 \in (0, 1)$.

G. Bartha and Thompson Modeling of Force Production

The Bartha and Thompson model of force production [24], [26] is a representation of muscle contraction based on the underlying (calcium) kinetics that activates the motor units. The full model consists of two parts: a model of isometric force production by a single motor unit; and a model of how the total isometric force for all motor units becomes dynamic whole muscle force, depending on the lumped properties of length and velocity. As we are modeling isometric muscle force data, we use only the first component of the model scaled by the number of motor units to become whole-muscle isometric force. The description of the Bartha and Thompson model presented here is taken from a reimplementation of the model described in [27].

The isometric component of the Bartha and Thompson model converts an arbitrary train of spikes into a time-varying isometric force. The model takes as input a Boolean value spike train $\mathbf{s} = (s_1, \ldots, s_N)$; each individual value $s_t = 0$ or 1 of the time-series of spikes denotes either the presence or absence of an action potential at sample time t. Each spike then affects the muscle by releasing an activating substance, some of which becomes bound by the muscle and thereby produces muscle force. Activator kinetics are represented in continuous-time by the following two equations derived from [37]

$$\dot{A}(t) = -k_1 \left(1 - \frac{B(t)}{B_m}\right) A(t) - k_2 \left(\frac{A(t)}{A(t) + A_{k_2}}\right) A(t) + \left(1 - \frac{A(t)}{A_m}\right) R(t) \tag{19}$$

$$\dot{B}(t) = k_1 \left(1 - \frac{B(t)}{B_m}\right) A(t) - k_3 \left(\frac{A_{k_3}}{A_{k_3} + A(t)}\right) B(t) \quad (20)$$

where $A(t)$ is the concentration of activator in the sarcoplasm that is available for binding, $B(t)$ is the concentration of activator bound to the myofilaments, k_1, k_2, and k_3 are rate constants, and A_{k_2}, A_{k_3}, A_m, and B_m are constants introducing various saturating nonlinearities into the system. The term $R(t)$ describes the release of activator by action potentials delivered at $t_i = t_1, t_2, \ldots$

$$R(t) = \sum_i A_b f\left(t_{\text{ipi}}[i]\right) \delta(t - t_i) \quad (21)$$

$$t_{\text{ipi}}[i] = t_i - t_{i-1} \quad (22)$$

$$f(t_{\text{ipi}}) = 1 + f_{\max} \left(\frac{t_{\text{ipi}}[i]}{t_{\max}}\right)^2 \exp\left[2\left(1 - \frac{t_{\text{ipi}}[i]}{t_{\max}}\right)\right] \quad (23)$$

where A_b is the baseline level of activator release (i.e., with no facilitation), $t_{\text{ipi}}[i]$ is the time interval between two neighboring spike stimuli, and $f_{\max}$ and $t_{\max}$ parameterize a nonlinear "facilitation" factor $f(t_{\text{ipi}})$, which is a function of the interpulse interval t_{ipi}. The isometric force $f(t)$ exerted by a motor unit is proportional to the concentration of bound activator $f(t) = cB(t)$, where c is an empirically determined constant for a single motor unit. Then whole muscle isometric force

$$y(t) = CB(t) \quad (24)$$

is the single unit isometric force $f(t)$ scaled by the total number of number of motor units n, which is included in the constant $C = nc$.

Model parameters were estimated using the Nelder–Mead simplex method, as for the Bobet and Stein model. The model description required the use of the raw spike train as input; therefore, the model output was resampled to 500 Hz after simulation for the purpose of fitting to the FL71 data. The parameters were initialized using the estimates from optimized values [27, Table II] for retractor bulbi muscle.

H. Nonlinear Input–output Modeling of Force Production

The deterministic NARX model is a general dynamic descriptor of discrete-time nonlinear systems [30]

$$\begin{aligned} y_t &= l(y_{t-1}, \ldots, y_{t-n_y}, u_{t-1-d}, \ldots, u_{t-n_u-d}) \\ &= l(\boldsymbol{\psi}_t) \end{aligned} \quad (25)$$

where $\boldsymbol{\psi}_t = \left[y_{t-1}, \ldots, y_{t-n_y}, u_{t-1-d}, \ldots, u_{t-n_u-d}\right]$ and $l(.)$ is a nonlinear function. The nonlinear function $l(.)$ is typically described by a set of weighted basis functions, such as polynomials, wavelets or radial basis functions. Here, the input–output signals (in the NARX model) were transformed by polynomial basis functions $\phi_j(.)$, so that the system output was represented by the model

$$y_t = \sum_{j=1}^{n_m} w_j \phi_j(\boldsymbol{\psi}_t) \quad (26)$$

where $w_j \in \mathbb{R}$ is an NARX model parameter and n_m is the number of basis functions used to describe the system.

Structure detection for the polynomial NARX model involves determining a number of parameters: the polynomial order n_p, the dynamic orders n_y and n_u, and the number of basis functions n_m to include in the model description. In general, a search-space of L possible basis functions is defined based on forming all the polynomial terms possible from the parameters n_p, n_y, and n_u. Then, the basis functions are selected from this superset [38].

It is helpful to include prior information to simplify the structure detection procedure at the outset [39]. Hence, we fixed the dynamic order of the model n_y using the results obtained from the linear dynamic modeling (i.e., $n_y = 2$, see Section III), similar to [40]. In addition, we used the prior information of the saturation effect shown in Fig. 3(a), to hypothesize that the force curves would be well described by either a quadratic or cubic function. Hence, we restricted this investigation to a comparison of linear, quadratic and cubic polynomial models, i.e., $n_p = 1, 2, 3$ (where $n_p = 1$ corresponds to the linear case, described earlier).

In principle, the basis functions of the NARX model can be detected using a forward regression method such as the forward-regression orthogonalization (FRO) algorithm [41], which is computationally efficient for selecting models from large initial sets of basis functions. In practice, we found that application of the FRO algorithm gave relatively poor model fits (based on visual inspection of the resulting model simulation). Related problems in using the FRO algorithm (selection of suboptimal models) have been noted elsewhere [42], inspiring various modifications [43], [44]. Hence, for structure detection, here we took advantage of the low model order to conduct an exhaustive hierarchical search, which ordered the model terms by significance. Specifically, the set of selected model terms M was iteratively ordered by: 1) evaluating each unselected term's contribution to reducing the SSE; 2) selecting the term corresponding to the minimum SSE; and then 3) repeating for the remaining terms. The SSE was obtained from numerical minimization of the output error cost function $F = \sum_{t=1}^{N} (y_t - \hat{y}_t)^2$ w.r.t. the NARX model parameters, where $\hat{y}_t$ was the NARX model prediction.[2] Cost function minimization was performed using the Nelder–Mead simplex method (implemented in MATLAB by the function *fminsearch*) and parameters were initialized using least squares. The structure-detection procedure is described in Algorithm 1.

Algorithm 1 is computationally slower than FRO but is feasible in this case because of the small search space (i.e., because the model orders n_y, n_u, and n_p are small). This approach is related to that of [45], who reported that use of the simulated prediction error, rather than one-step-ahead errors (as used in FRO), can lead to improved model selection.

A preliminary investigation using the FRO algorithm showed that the linear terms y_{t-1}, y_{t-2}, and u_{t-1} consistently dominated structure selection. Hence, to initialize the structure-detection

[2]This method of estimating the model parameters assumes an output error framework, hence the resulting nonlinear model would more correctly be called a nonlinear output error (NOE) model [29]. However, we retain the more familiar NARX label for simplicity.

Algorithm 1 Structure detection procedure for the NARX model

$\mathcal{M}$ = Unordered set of all L model terms
M = Ordered set of initial selected model terms
$M^c = \mathcal{M} \setminus M$ {Ordered set of unselected terms}
for $j = 1$ to L **do**
  for $i = 1$ to $L - j + 1$ **do**
    $M_{\text{Test}} = M \cup M_i^c$ {Include the i^{th} element of M^c in the test model}
    $\text{SSE}_i = \min[F(M_{\text{Test}})]$ {Evaluate the sum-of-squared error (SSE) for model M_{Test} using cost function $F(.)$}
  end for
  k = index[min(SSE)] {Find the index of the model term corresponding to the minimum in the SSE vector}
  $M = M \cup M_k^c$ {Add chosen term to the model set}
  $M^c = M^c \setminus M_k^c$ {Remove chosen term from the model set complement}
end for

procedure in Algorithm 1, we fixed the initial model M as these same linear terms. The set of model terms M produced by Algorithm 1 was an ordered set of all terms (ordered by significance). To obtain a parsimonious description, we truncated these ordered terms by visual inspection of the SSE curve, and thereby fixed the final number of model terms n_m.

III. Results

A. Features of Nonlinearity

The need for nonlinear modeling of the force curves is clearly shown by a preliminary analysis. The dataset used here comprises force signals recorded from constant stimulation frequency inputs. Therefore, the saturation effect on force magnitude can be observed by plotting the stimulation frequency versus peak force directly from the data, shown in Fig. 3(a). The saturation effect is modeled in Fig. 3(a) by a sigmoidal function of the form given in (6), which produces a good fit.

In addition, the output of a linear system to a constant input, when normalized by the magnitude of the response at a fixed-time point, should be the same for different magnitudes of the input (assuming initial conditions are zero). Therefore, we normalized the FL71 force profiles by each response magnitude at 120 ms; this revealed that the rate of response increased with stimulation frequency, shown in Fig. 3(b).[3] Whereas the saturation effect appears to be a static nonlinearity, the varying rate of response revealed in Fig. 3(b) suggests that there is also a dynamic nonlinearity in the muscle dynamics.

Last, the time constants in the activation portion of the force responses do not appear to be the same as the decay portion, excepting the high frequency of stimulation at 500 Hz [see Fig. 3(c)]. This implies that a linear model would not fit the data well at individual lower frequencies of stimulation. Another striking feature of the decay curves is that, unlike the activation curves, the time constants appear similar across all responses.

[3]For the illustration in Fig. 3(b), each force profile was smoothed by application of a forward-backward pass of a Butterworth filter (fifth-order, cutoff frequency 50 Hz), in order to remove the oscillatory features in the 100 Hz response and provide a more effective visual comparison.

B. Linear Modeling Results

The 2 pole 1 zero model structure has been shown to give good fits to oculomotor muscle force [33], [34]. However, those results were obtained from fitting single responses. Here, we also found that fitting separate models to individual force curves gave reasonable results at high frequency [see Fig. 4(a)]. At low frequency, the fits were poor due to the fact that activation and decay time constants were apparently different (as mentioned earlier).

When the 2 pole 1 zero model was fitted across the entire set of force curves, the results degraded. In accordance with a saturation effect, the linear model over-predicted the amplitude of the 100 Hz and 500 Hz force curves and under-predicted the 200 and 300 Hz force curves, which is shown in Fig. 4(b). The linear model had a variance accounted for (VAF) $= 0.888$. The 2 pole 1 zero model was fitted to the stimulation section only because fitting to the entire duration of each force signal resulted in an unstable model. In addition, the FIR model (of order $n_b = 30$, chosen to be high order where the response had decayed to zero) gave similar fits to the 2 pole 1 zero model [see Fig. 4(c)], which implied that more complex, higher order models would not give any significant improvement (the VAF of the FIR model was 0.898).

C. Wiener and Cascaded Wiener Modeling Results

We fitted the Wiener model using both a transfer function to describe the dynamics and a high-order FIR model. For the transfer function approach, following on from the linear modeling, we used a 2 pole 1 zero dynamic model in combination with a sigmoidal function as described in Section II. For the FIR approach, we fitted a model of order $n_b = 30$, with a third-order polynomial as the static nonlinearity (which we also compared against higher order polynomials with no significant improvement). Each model was comparable in accuracy (VAFs of 0.965 and 0.953 for the transfer function and FIR cases, respectively). Both Wiener models gave improved results compared to the linear model in terms of describing the saturation but did not accurately describe the dynamics (results not shown). We extended the FIR Wiener model by adding in parallel cascades, where in each cascade the FIR model was of order $n_b = 30$ and the polynomial was of third order. We added in additional cascades until the sum-of-squared error began to flatten, which took six cascades. We found that this improved the results in terms of increasing the fit accuracy (VAF $= 0.994$). However, the disadvantage was that there were a large number of parameters in the resulting model (34 parameters in each cascade, resulting in a total of 204 parameters for the complete model). In addition, the model was not smooth in the response unlike the subsequent nonlinear models that we fitted [shown in Fig. 5(a)]. Potentially, this problem could have been resolved via regularization, however, with such a large number of parameters in the model this proved difficult to achieve without degrading the fit. Due to the

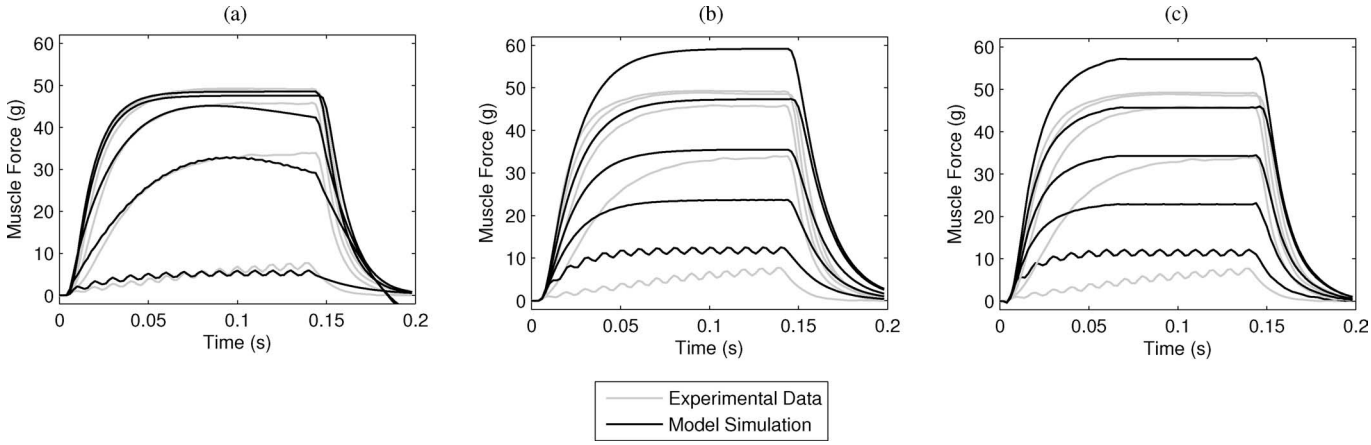

Fig. 4. Linear model simulations in comparison to experimental recordings of muscle force. (a) Separate linear models for each frequency of stimulation. (b) Single linear model, where the structure is 2 pole 1 zero. (c) Single linear model, where the structure is FIR.

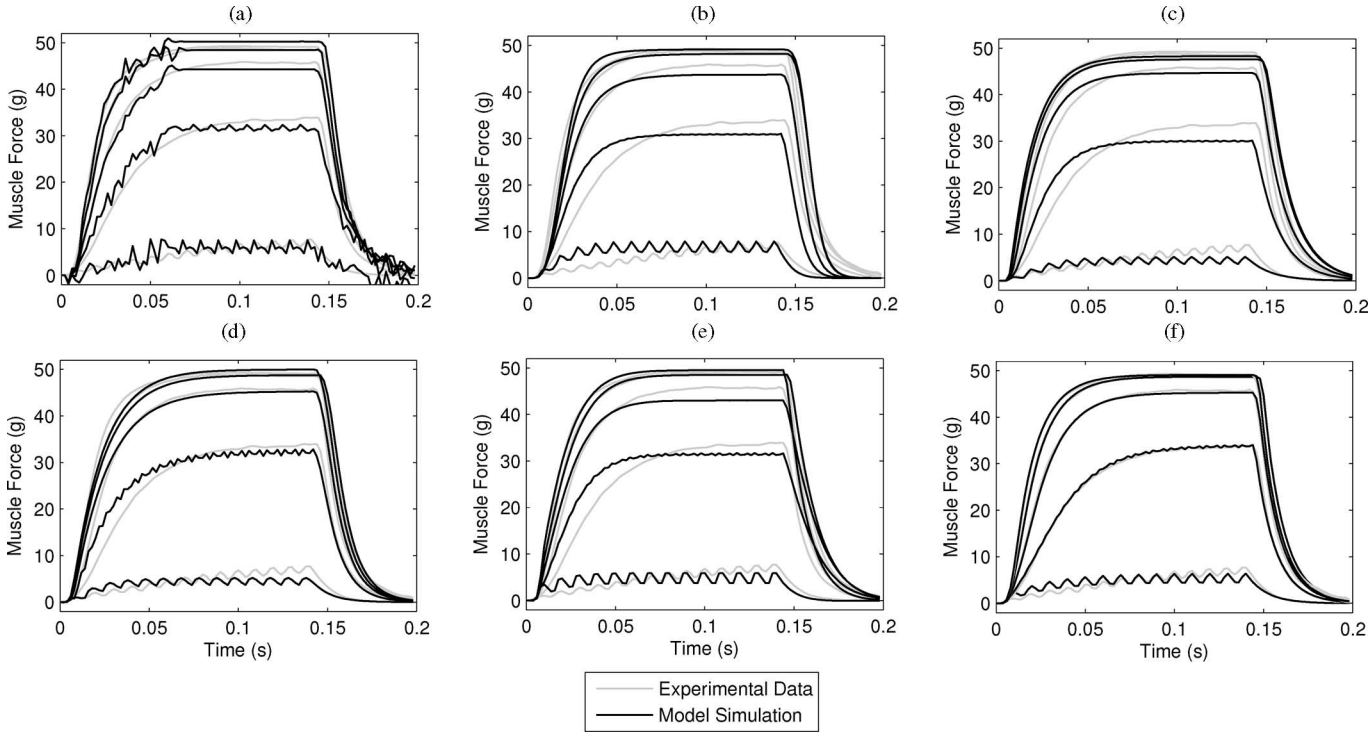

Fig. 5. Nonlinear model simulations in comparison to experimental recordings of muscle force. (a) Parallel cascade model. (b) VM model. (c) Bobet and Stein model. (d) Bartha and Thompson model. (e) Quadratic NARX model. (f) Cubic NARX model.

large complexity of the model, we did not pursue this line of investigation further.

D. VM Modeling Results

The activation function in the VM model represents a static nonlinearity, originally derived from observations of saturation in mammalian skeletal muscle [46], and therefore, similar in functional form to the saturation effect observed here [compare [46, Fig. 4] with Fig. 3(a)]. The model structure of second-order dynamics followed by a static-saturation function is very similar to the 2 pole 1 zero Wiener model discussed earlier. The VAF of the VM model was 0.982 and so improved on the Wiener model. The VM model was not as accurate as the parallel cascade model but had reduced complexity and gave a smoother output, qualitatively more similar in form to the true data [simulation of the VM model shown in Fig. 5(b)].

E. Bobet and Stein Modeling Results

The structure of the Bobet and Stein model was predefined, and hence, only the parameters were adjusted here, by nonlinear estimation. The time constant of the input filter (representing calcium dynamics) was estimated as 7.1 ms, which is fast, reflecting the rapid rise of force in the rectus muscle. The order of the nonlinearity n was estimated to be 4.8. This is higher than

TABLE I
MODEL TERMS WITH CORRESPONDING PARAMETER ESTIMATES AND VARIANCES FOR A SUBSET OF THE IDENTIFIED MODELS

	Term	Param.	Param. Est. (Var.)
VM Model	-	T_{f1}	7.932 $\times 10^{-3}$ (1.92 $\times 10^{-8}$)
	-	T_{f2}	9.192 $\times 10^{-3}$ (3.36 $\times 10^{-7}$)
	-	T_{f3}	2.887 $\times 10^{-2}$ (1.30 $\times 10^{-5}$)
	-	T_{f4}	1.051 $\times 10^{-2}$ (1.46 $\times 10^{-6}$)
	-	a_f	0.1848 (2.15 $\times 10^{-4}$)
	-	n_f	1.931 (3.76 $\times 10^{-3}$)
Bobet and Stein Model	-	a_1	0.7530 (9.77 $\times 10^{-5}$)
	-	n	4.781 (1.44 $\times 10^{-2}$)
	-	k_0	1.464 (3.41 $\times 10^{-3}$)
	-	b_0	77.47 (5.03)
	-	b_1	3.032 $\times 10^{-5}$ (7.98 $\times 10^{-10}$)
	-	B	45.07 (8.21 $\times 10^{-2}$)
Bartha and Thomp. Model	-	k_1	97.68 (1.69)
	-	k_2	305.8 (11.6)
	-	k_3	101.4 (3.09)
	-	c	62.06 (0.129)
	-	A_m	2.572 (2.86 $\times 10^{-2}$)
	-	B_m	0.9942 (8.39 $\times 10^{-5}$)
	-	A_b	9.302 $\times 10^{-2}$ (5.08 $\times 10^{-7}$)
	-	A_{k_2}	2.376 $\times 10^{-4}$ (2.32 $\times 10^{-10}$)
	-	A_{k_3}	8.072 $\times 10^{-2}$ (5.64 $\times 10^{-6}$)
	-	f_m	5.082 (2.42 $\times 10^{-3}$)
	-	t_m	3.825 $\times 10^{-3}$ (2.96 $\times 10^{-9}$)
Quad. NARX Model	y_{t-1}	w_1	1.6722 (5.96 $\times 10^{-6}$)
	y_{t-2}	w_2	-0.70100 (3.68 $\times 10^{-6}$)
	u_{t-3}	w_3	0.60582 $\times 10^{-3}$ (1.26 $\times 10^{-7}$)
	u_{t-4}^2	w_4	-3.3251 $\times 10^{-5}$ (9.47 $\times 10^{-13}$)
	$u_{t-3}u_{t-4}$	w_5	2.6848 $\times 10^{-5}$ (9.45 $\times 10^{-13}$)
Cubic NARX Model	y_{t-1}	w_1	1.1966 (1.12 $\times 10^{-5}$)
	y_{t-2}	w_2	-0.30353 (5.69 $\times 10^{-6}$)
	u_{t-3}	w_3	2.1884 $\times 10^{-3}$ (6.78 $\times 10^{-8}$)
	u_{t-3}^3	w_4	9.9258 $\times 10^{-9}$ (7.39 $\times 10^{-19}$)
	$y_{t-1}u_{t-3}$	w_5	2.3645 $\times 10^{-3}$ (1.38 $\times 10^{-10}$)
	$y_{t-1}^2u_{t-3}$	w_6	-3.2171 $\times 10^{-5}$ (5.97 $\times 10^{-14}$)
	$y_{t-2}u_{t-3}^2$	w_7	2.1518 $\times 10^{-6}$ (1.10 $\times 10^{-15}$)
	$y_{t-2}^2u_{t-3}$	w_8	2.3126 $\times 10^{-5}$ (1.06 $\times 10^{-14}$)
	$y_{t-2}u_{t-3}$	w_9	-1.4618 $\times 10^{-3}$ (5.96 $\times 10^{-11}$)
	$y_{t-1}u_{t-3}^2$	w_{10}	-2.8328 $\times 10^{-6}$ (4.46 $\times 10^{-16}$)

previously found in the muscle model of human ankle dorsiflexion [23], where n was in the range 3.1–3.6. The parameter b_1 was estimated as $b_1 = 3.032 \times 10^{-5}$, which caused the time-varying term in (15) to always be close to zero. Hence, the time-varying output filter was close to constant and could have been replaced by a time-invariant filter with little loss of accuracy (where the filter time constant would have been 12.9 ms, a function of b_0). All the Bobet and Stein model parameters are listed in Table I. The prediction accuracy of the Bobet and Stein model was high, with VAF = 0.985. A visual inspection of the model fits, shown in Fig. 5(c), shows that the rise of force does not exactly match the data, although the qualitative features of increasing rise time with stimulation frequency is described by the model, along with the saturation effect.

F. Bartha and Thompson Modeling Results

Similar to the Bobet and Stein model, the model structure was predefined, and hence only the parameters were adjusted here. Most of the parameters were of similar magnitude to their initialized values taken from a fit to retractor bulbi muscle [27]. The main difference from the previous fit was the value of the parameter C that determines the overall magnitude of the isometric force. The current value for lateral rectus muscle force is approximately one hundred times larger than for retractor bulbi single unit force data, mainly attributable to the difference in scaling between whole muscle and single unit forces. The overall behavior of the model depends on a complex interplay between the various parameters, making it difficult to associate a model feature with a specific parameter. Instead, we observe that the fitted values used here result in a single unit twitch response approximately half the amplitude of that for retractor bulbi muscle, as a proportion of maximal possible isometric force. Tetanic tension also increases more slowly with firing frequency than found previously, reaching its peak value in lateral rectus muscle at 400–500 Hz, as opposed to ~200 Hz for retractor bulbi muscle. Furthermore, the rise time to tetanus is roughly double that for retractor bulbi muscle, consistent with the smaller twitch response. A visual summary of the model fits, shown in Fig. 5(d), shows that the fitted force curves do not exactly match the data. However, qualitative features such as the change in rise time and maximal isometric force with stimulation frequency are captured well and are similar in fit quality to the Bobet and Stein model.

G. Polynomial NARX Modeling Results

The NARX model structure detection problem was focused on selecting a parsimonious set of model terms from a superset of possible basis functions. The dynamic order n_y was assumed to be second order, which was shown in the linear modeling to accurately describe the dynamics of individual force curves during stimulation. Two polynomial orders were investigated: quadratic and cubic, resulting in two separate NARX models. We studied the effect of varying the model parameter n_u for each NARX model (i.e., $n_u = 1$ and $n_u = 2$). We found that for the quadratic model setting $n_u = 1$ gave poor fits (results not shown). For the cubic model similar accuracy was obtained between setting $n_u = 1$ and $n_u = 2$ but $n_u = 1$ resulted in a smaller set of model terms ($n_m = 10$ for $n_u = 1$ and $n_m = 13$ for $n_u = 2$). The final model terms of each NARX model were selected by ordering the terms using Algorithm 1 and then truncating the model by visual inspection of the SSE curve, shown for each model in Fig. 6. The final selected NARX models had the following structure: 1) quadratic model $n_y = 2, n_u = 2, n_p = 2, n_m = 5$; and 2) cubic model $n_y = 2, n_u = 1, n_p = 3, n_m = 10$. The parameter estimates for the quadratic and cubic NARX models are given in Table I and the model simulations are shown in Fig. 5(e) and (f), respectively.

The quadratic NARX model had fewer terms relative to the cubic NARX model and similar high accuracy VAFs = 0.989 and 0.999, respectively. The striking feature of the quadratic NARX model was that it described the muscle force dynamics using only one nonlinear difference equation of five model terms with an accuracy similar to that of both the Bobet and Stein model (a time-varying model that uses six free parameters and six equations) and the Bartha and Thompson model (11 free parameters and 5 equations)—prediction accuracy of the models is compared directly in Fig. 7.

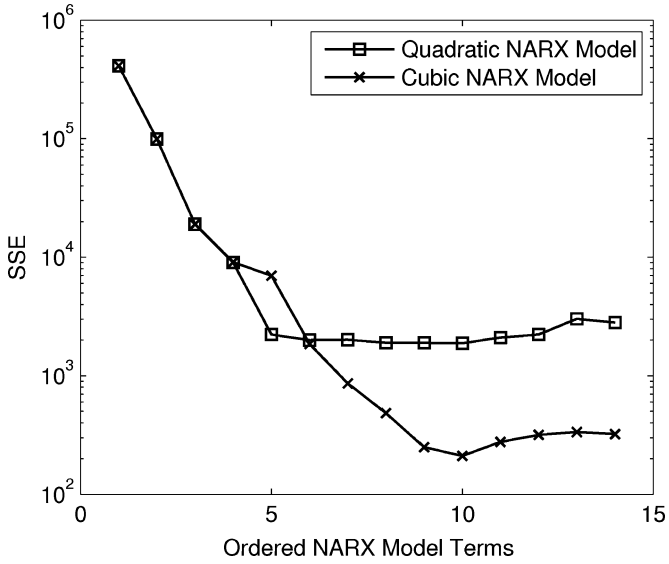

Fig. 6. Quadratic and cubic NARX models terms ordered by contribution to decreasing the SSE using Algorithm 1 (plot truncated at 14 terms for the cubic model).

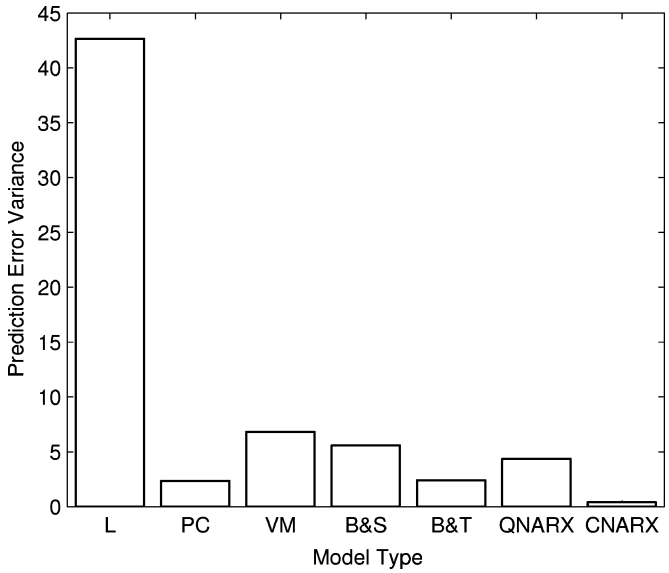

Fig. 7. Comparison of model accuracy in terms of prediction error variance, where labels on the horizontal axis refer to linear model (L), Parallel Cascade model (PC), Virtual Muscle model (VM), Bobet and Stein model (B&S), Bartha and Thompson model (B&T), quadratic NARX model (QNARX), and cubic NARX model (CNARX).

Finally, the results suggest that the most accurate model was the cubic NARX model, which improved on the fit accuracy of all the other models, with an associated increase in number of terms (ten terms in the cubic NARX model compared to five in the quadratic NARX model).

IV. Discussion

Nonlinearities in the oculomotor plant have only recently become the subject of systematic investigation [47]–[49], and are typically not included in models of eye movement control. Here, we attempted to model one particular source of plant nonlinearity, the relation between neural firing and isometric force in the lateral rectus muscle as described by Fuchs and Luschei [6]. We found that this relation could be well approximated by two different types of nonlinear model, one based on underlying physical processes, the other derived from a generic method for nonlinear plant identification (NARX) not previously used in the context of eye-movement control.

We discuss these findings first in relation to previous models of the oculomotor plant, then in connection with muscle modeling in general, and finally for their implications for future work on oculomotor control.

A. Oculomotor Plant Models

The relationship between changes in motoneuron firing rate and force production has been given relatively little attention in previous models of the oculomotor plant. Although Robinson [20] discussed in general terms the nonlinearities considered here, specific models have tended to use linear approximations either explicitly (e.g., [50]–[52]), or implicitly in lumped equations relating motoneuron firing-rate to eye-movements themselves [8]. To our knowledge, there has been no previous attempt to model isometric force production as measured by Fuchs and Luschei [6].

The striking inadequacy of a single linear model for fitting these data (see Figs. 4 and 7) seems puzzlingly incompatible with the general success of linear models in oculomotor control as a whole. However, there are a number of reasons why the force-production nonlinearity would not have been apparent in previous studies, and these throw light on its general significance for understanding oculomotor control.

First, a number of studies have focused on the mechanical portion of the oculomotor plant (see Fig. 1), that is the relation between the force applied to the globe and orbital tissues, and the resultant eye displacement [7]–[9], [33], [34], [53], [54]. It appears that this relation can be well approximated by a linear model for a significant part of the normal operating range. The contrast between linear and nonlinear portions of the plant are particularly visible in the effects of stimulation of the abducens nucleus in awake primates [5]. During and immediately after stimulation, eye-displacement is nonlinearly related to stimulation frequency in a manner similar to that described for isometric force [6]. After stimulation, when the neural signals to the lateral rectus are assumed to be unchanging, the return movements of the eye to its initial position can be well described by a linear model of plant mechanics [5]. Thus, oculomotor plant nonlinearities are to some extent confined to a portion of the plant, namely the processes converting neural input to muscle force (see Fig. 1).

Second, even when the entire plant is considered, these nonlinearities need not become apparent if only a limited range of eye-movements are being modeled. This can be seen in the present study, where the effects of a single stimulation frequency can be reasonably well fitted by a linear model specific to that frequency (see Fig. 4). Similarly, the relation between motoneuron firing rate and eye displacement can be approximated by separate linear models, each for a restricted range

of eye-movement velocities [4]. It seems likely that the linear equations relating motoneuron discharge to eye displacement found in the literature (e.g., [10], [55]–[57]) are at least in part due to their dealing with a restricted range of eye movements.

Finally, it has been shown in a much simpler control system that nonlinearities similar to those modeled here can be consistent with an overall linear relation between plant input and output, provided motoneurons are recruited appropriately [27], [28], [58]. A detailed distributed model of the nictitating membrane response, based on the earlier work of Bartha and Thompson [24], [26], incorporated a model of the retractor bulbi muscle (see Section II) with nonlinearities derived from the measurements of isometric force in individual motor units [59], which were very similar to those described here. Yet appropriate combinations of recruitment and rate coding could be shown to give an almost linear relation between total firing rate of the motoneuron pool and simulated nictitating-membrane displacement [27], a relation that subsequent EMG analysis suggested was achieved in practice [28]. If motoneuron firing were organized similarly for eye-movements, then the oculomotor plant would appear effectively linear to premotor structures and linear relationships between the firing rates of premotor neurons and eye displacement could be observed (e.g., [60]–[64]).

B. General Muscle Models of Isometric Force Production

Previous modeling studies of the relation between muscle stimulation and isometric force have primarily concerned skeletal and cardiac muscle. The nonlinear dynamic processes involved in force production are known to include the release of calcium from the sarcoplasmic reticulum, calcium kinetics within the sarcoplasm, the interaction of calcium with troponin and hence cross-bridge formation, and the effects of cross-bridge formation on intrinsic muscle viscoelasticity (e.g., [65]). These processes are very complex, and there is no generally accepted model that relates them to overall muscle behavior (references in [27]). There are instead a large number of models available, which range from very detailed biological models that have many parameters but reflect underlying processes, to "black-box" models with few parameters but no explicit relation to underlying processes (e.g., [66]–[68]).

The present study focused on the simpler end of this spectrum (though it should be noted that the Bartha and Thompson model has been shown to be compatible with a detailed cross-bridge formulation [28]). Its main contribution is to show that nonlinear system identification can be applied successfully to the problem of isometric force production in eye muscle, giving fits to the data at least as good as those derived from approximations to physically based nonlinear dynamics (see Figs. 5 and 7). Although the nonlinear system identification approach has been applied extensively to engineered systems, it has received limited attention for muscle modeling [40], [69], [70]. To our knowledge, the NARX-type identification of muscle dynamics has never been compared and benchmarked against existing biophysical models.

It is clear from Fig. 5 that the quadratic NARX model [see Fig. 5(e)] has a pattern and magnitude of errors similar to that of the VM, Bobet and Stein, and Bartha and Thompson models (see Fig. 5(b)–(d)], for example, all these models fail to predict the slow rise time at intermediate stimulation frequencies. This suggests that the cubic NARX model, which does capture this behavior, models important system dynamics, which is missing from the other models, while retaining a relatively simple model description (ten parameters compared to, e.g., six in the case of the Bobet and Stein model). Although the quadratic NARX model was found to mimic (input) static nonlinearities, similar to terms that might be obtained from a (polynomial) generalized Hammerstein model, the modeling procedure did not lead to selection of cross-product input–output terms representing essentially dynamic nonlinearities (such as dissipation with quadratic dependence on state variables). Our results indicate that capturing such dynamic nonlinearities will be important for accurate modeling of force production. It also indicates that the nonlinear processes present in the biophysically based models we consider (VM model, Bobet and Stein, and Bartha and Thompson) are inadequate to describe force production at varying stimulus frequency. It would be of great interest to understand the biophysical origin of the additional dynamic nonlinearities, which are required.

C. Future Models of Oculomotor Control

The study by Fuchs and Luschei [6] is one of the few investigations into the dynamics of force production in eye muscle. However, these data were not collected under conditions designed for the application of system identification techniques. Due to this, the data were not so useful for discriminating between different types of model—the nonlinear models investigated here all gave high VAFs, presumably because the fit error was dominated by the steady-state portion of the response (which was well described by each model). Therefore, while the models constructed here are useful as a formative investigation into the isometric nonlinearities of the primate extraocular muscles, it is clear that further data are required to improve computational descriptions in the future, as also emphasized in [47].

It was suggested earlier that appropriate recruitment of ocular motoneurons might present premotor structures with an oculomotor plant that appeared linear. Investigating this possibility in simulation requires the use of distributed models, in which individual ocular motoneurons and their muscle units are represented explicitly. Previous application of such a model to the control of static eye position suggests that in this simple case appropriate recruitment can indeed linearize the plant: although the active muscle force required to maintain the eye in a fixed position varies nonlinearly with eye position in the orbit, this can be achieved by recruitment of motor units of different strengths, each of which fires linearly with eye-position above its recruitment threshold [71].

How far oculomotor plant dynamics can be linearized in similar fashion could be explored by a distributed model that was extended to include the dynamic behavior of motor units. As noted earlier, a distributed model has been used for the dynamics of the nictitating membrane response [24], [26]–[28], and

it appears from the present results that its basic representation of force-production nonlinearities in the retractor bulbi muscle could be appropriately parameterized for primate extraocular muscles. Alternatively, the present work indicates individual motor units could be compactly represented by NARX functions. Data for individual motor units in rotatory extraocular muscles may help decide this issue [14], [72]. The model would also need to take into account additional sources of nonlinearity, such as the interaction between muscle activation, length and velocity, and the control signal to the antagonist muscle falling to zero, as it does for certain saccades [4].

The difficulties inherent in nonlinear control [73] point to the potential importance of plant linearization in biological systems [74], [75]. Understanding plant linearization in the relatively simple case of oculomotor control may throw light on any similar principles that are used for skeletal muscles.

REFERENCES

[1] D. Robinson, "Is the oculomotor system a cartoon of motor control?" in *Oculomotor and Skeletal Motor System: Differences and Similarities* (ser. Progress in Brain Research), vol. 64. H.-J. Freund, U. Bttner, B. Cohen, and J. Noth, Eds. Amsterdam, The Netherlands: Elsevier, 1986, pp. 411–417.

[2] D. T. Westwick and R. E. Kearney, *Identification of Nonlinear Physiological Systems*. New York: Wiley, 2003.

[3] R. H. S. Carpenter, *Movements of the Eyes*, 2nd ed. London, U.K.: Pion, 1988.

[4] P. A. Sylvestre and K. E. Cullen, "Quantitative analysis of abducens neuron discharge dynamics during saccadic and slow eye movements," *J. Neurophysiol.*, vol. 82, pp. 2612–2632, 1999.

[5] S. R. Anderson, J. Porrill, S. Sklavos, N. J. Gandhi, D. L. Sparks, and P. Dean, "Dynamics of primate oculomotor plant revealed by effects of abducens microstimulation," *J. Neurophysiol.*, vol. 101, pp. 2907–2923, 2009.

[6] A. Fuchs and E. Luschei, "Development of isometric tension in simian extraocular muscle," *J. Physiol.*, vol. 219, no. 1, pp. 155–166, 1971.

[7] D. A. Robinson, "The mechanics of human saccadic eye movement," *J. Physiol.*, vol. 174, pp. 245–264, 1964.

[8] S. Sklavos, J. Porrill, C. R. S. Kaneko, and P. Dean, "Evidence for wide range of time scales in oculomotor plant dynamics: Implications for models of eye movement control," *Vis. Res.*, vol. 45, pp. 1525–1542, 2005.

[9] S. Sklavos, D. M. Dimitrova, S. J. Goldberg, J. Porrill, and P. Dean, "Long time-constant behaviour of the coulomotor plant in barbiturate anesthetized primate," *J. Neurophysiol.*, vol. 95, no. 2, pp. 774–782, 2006.

[10] R. Ramachandran and S. G. Lisberger, "Transformation of vestibular signals into motor commands in the vestibuloocular reflex pathways of monkeys," *J. Neurophysiol.*, vol. 96, pp. 1061–1074, 2006.

[11] G. Asmussen and U. Gaunitz, "Mechanical properties of the isolated inferior oblique muscle of the rabbit," *Pflugers Arch.*, vol. 392, pp. 183–190, 1981.

[12] N. H. Barmack, C. C. Bell, and B. G. Rence, "Tension and rate of tension development during isometric responses of extraocular muscle," *J. Neurophysiol.*, vol. 34, pp. 1072–1079, 1971.

[13] K. N. Bishop, J. R. McClung, S. J. Goldberg, and M. S. Shall, "Anatomic and physiological characteristics of the ferret lateral rectus muscle and abducens nucleus," *J. Appl. Physiol.*, vol. 103, no. 5, pp. 1706–1714, 2007.

[14] S. J. Goldberg, M. A. Meredith, and M. S. Shall, "Extraocular motor unit and whole-muscle responses in the lateral rectus muscle of the squirrel monkey," *J. Neurosci.*, vol. 18, no. 24, pp. 10 629–10 639, 1998.

[15] J. Stelling and A. McVean, "The contractile properties and movement dynamics of pigeon eye muscle," *Pflugers Arch.*, vol. 412, pp. 314–321, 1988.

[16] Y. Yamanaka and P. Bach-y Rita, "Relations between extraocular muscle contraction and extension times in each phase of nystagmus," *Exp. Neurol.*, vol. 27, no. 1, pp. 57–65, 1970.

[17] I. Brown and G. Loeb, "Measured and modeled properties of mammalian skeletal muscle: IV. Dynamics of activation and deactivation," *J. Muscle Res. Cell Motil.*, vol. 21, no. 1, pp. 33–47, 2000.

[18] A. Buller and D. Lewis, "The rate of tension development in isometric tetanic contractions of mammalian fast and slow skeletal muscle," *J. Physiol. (Lond.)*, vol. 176, pp. 337–354, 1965.

[19] S. Cooper and J. C. Eccles, "The isometric responses of mammalian muscles," *J. Physiol. (Lond.)*, vol. 69, pp. 377–385, 1930.

[20] D. Robinson, "Models of the mechanics of eye movements," in *Models of Oculomotor Behaviour*, B. Zuber, Ed. Boca Raton, FL: CRC Press, 1981, pp. 21–41.

[21] P. Dean and J. Porrill, "Adaptive filter models of the cerebellum: computational analysis," *Cerebellum*, vol. 7, pp. 567–571, 2008.

[22] M. J. Korenberg, "Parallel cascade identification and kernel estimation for nonlinear systems," *Ann. Biomed. Eng.*, vol. 19, no. 4, pp. 429–455, 1991.

[23] J. Bobet, E. R. Gossen, and R. B. Stein, "A comparison of models of force production during stimulated isometric ankle dorsiflexion in humans," *IEEE Trans. Neural Syst. Rehabil. Eng.*, vol. 13, no. 4, pp. 444–451, Dec. 2005.

[24] G. T. Bartha and R. F. Thompson, "Control of rabbit nictitating membrane movements: I. A computer model of the retractor bulbi muscle and the associated orbital mechanics," *Biol. Cybern.*, vol. 68, no. 2, pp. 135–143, 1992.

[25] D. Song, G. Raphael, N. Lan, and G. E. Loeb, "Computationally efficient models of neuromuscular recruitment and mechanics," *J. Neural Eng.*, vol. 5, pp. 175–184, 2008.

[26] G. T. Bartha and R. F. Thompson, "Control of rabbit nictitating membrane movements. II. Analysis of the relation of motoneuron activity to behavior," *Biol. Cybern.*, vol. 68, no. 2, pp. 145–154, 1992.

[27] E. Mavritsaki, N. Lepora, J. Porrill, C. H. Yeo, and P. Dean, "Response linearity determined by recruitment strategy in detailed model of nictitating membrane control," *Biol. Cybern.*, vol. 96, no. 1, pp. 39–57, 2007.

[28] N. F. Lepora, E. Mavritsaki, J. Porrill, C. H. Yeo, C. Evinger, and P. Dean, "Evidence from retractor bulbi EMG for linearised motor control of conditioned nictitating membrane responses," *J. Neurophysiol.*, vol. 98, pp. 2074–2088, 2007.

[29] O. Nelles, *Nonlinear System Identification*. Berlin, Germany: Springer-Verlag, 2001.

[30] I. J. Leontaritis and S. A. Billings, "Input-output parametric models for non-linear systems part 1: Deterministic nonlinear systems," *Int. J. Control*, vol. 2, pp. 303–328, 1985.

[31] L. Ljung, *System Identification—Theory for the User*, 2nd ed. Upper Saddle River, NJ: Prentice-Hall, 1999.

[32] L. Ljung, "Initialisation aspects for subspace and output error identification methods," presented at the 5th Eur. Control Conf., Cambridge, U.K., 2003.

[33] H. Goldstein and R. Reinecke, "Clinical applications of oculomotor plant models," *Contemporary Ocular Motor and Vestibular Research: A Tribute to David A. Robinson; International Meeting, Eibsee 1993*, A. Fuchs, T. Brandt, U. Bttner, and D. Zee, Eds., Stuttgart, Georg Thieme Verlag, pp. 10–17, 1994.

[34] H. P. Goldstein, C. J. Bockish, and J. M. Miller, "Muscle forces underlying saccades," *Invest. Ophthalmol. Vis. Sci.*, vol. 41, no. 4, pp. S315–S315, 2000.

[35] B. Efron, "Bootstrap methods: Another look at the jackknife," *Ann. Statist.*, vol. 7, pp. 1–26, 1979.

[36] J. Bobet and R. B. Stein, "A simple model of force generation by skeletal muscle during dynamic isometric contractions," *IEEE Trans. Biomed. Eng.*, vol. 45, no. 8, pp. 1010–1016, Aug. 1998.

[37] R. B. Stein and E. Y.-M. Wong, "Analysis of models for the activation and contraction of muscle," *J. Theor. Biol.*, vol. 46, pp. 307–327, 1974.

[38] R. Haber and H. Unbehauen, "Structure identification of nonlinear dynamic systems - a survey on input/output approaches," *Automatica*, vol. 26, pp. 651–667, 1990.

[39] J. Sjoberg, Q. Zhang, L. Ljung, A. Benveniste, B. Delyon, P. Glorennec, H. Hjalmarsson, and A. Juditsky, "Nonlinear black box modeling in system identification: a unified overview," *Automatica*, vol. 31, no. 12, pp. 1691–1724, 1995.

[40] H. Gollee and K. J. Hunt, "Nonlinear modelling and control of electrically stimulated muscle: A local model network approach," *Int. J. Control*, vol. 68, no. 6, pp. 1259–1288, 1997.

[41] S. Chen, S. A. Billings, and W. Luo, "Orthogonal least squares methods and their application to non-linear system identification," *Int. J. Control*, vol. 50, pp. 1873–1896, 1989.

[42] A. Shertinsky and R. W. Picard, "On the efficiency of the orthogonal least squares training method for radial basis function networks," *IEEE Trans. Neural Netw.*, vol. 7, no. 1, pp. 195–200, Jan. 1996.
[43] K. Z. Mao and S. A. Billings, "Algorithms for minimal model structure detection in nonlinear dynamic system identification," *Int. J. Control*, vol. 68, no. 2, pp. 311–330, 1997.
[44] K. Li, J.-X. Peng, and E.-W. Bai, "A two-stage algorithm for identification of nonlinear dynamic systems," *Automatica*, vol. 42, pp. 1189–1197, 2006.
[45] L. Piroddi and W. Spinelli, "An identification algorithm for polynomial NARX models based on simulation error minimization," *Int. J. Control*, vol. 76, no. 17, pp. 1767–1781, 2003.
[46] I. E. Brown, E. J. Cheng, and G. E. Loeb, "Measured and modeled properties of mammalian skeletal muscle. II. The effects of stimulus frequency on force-length and force-velocity relationships," *J. Muscle Res. Cell Motil.*, vol. 20, pp. 627–643, 1999.
[47] C. Quaia, H. S. Ying, A. M. Nichols, and L. M. Optican, "The viscoelastic properties of passive eye muscle in primates. I: Static forces and step responses," *PLoS One*, vol. 4, no. 4, p. e4850, 2009.
[48] C. Quaia, H. S. Ying, and L. M. Optican, "The viscoelastic properties of passive eye muscle in primates. II: Testing the quasi-linear theory," *PLoS One*, vol. 4, no. 8, p. e6480, 2009.
[49] L. Yoo, H. Kim, V. Gupta, and J. L. Demer, "Quasilinear viscoelastic behavior of bovine extraocular muscle tissue," *Invest. Ophthalmol. Vis. Sci.*, vol. 50, no. 8, pp. 3721–3728, 2009.
[50] S. Lehman and L. Stark, "Simulation of linear and nonlinear eye movement models: Sensitivity analyses and enumeration studies of time optimal control," *J. Cybern. Inf. Sci.*, vol. 4, pp. 21–43, 1979.
[51] J. D. Enderle, E. J. Engelken, and R. N. Stiles, "A comparison of static and dynamic characteristics between rectus eye muscle and linear muscle model predictions," *IEEE Trans. Biomed. Eng.*, vol. 38, no. 12, pp. 1235–1245, Dec. 1991.
[52] K. D. Pfann, E. L. Keller, and J. M. Miller, "New models of the oculomotor mechanics based on data obtained with chronic muscle force transducers," *Ann. Biomed. Eng.*, vol. 23, pp. 346–358, 1995.
[53] D. Robinson, "The mechanics of human smooth pursuit eye movement," *J. Physiol.*, vol. 180, pp. 569–591, 1965.
[54] S. Seidman, R. Leigh, R. Tomsak, M. Grant, and L. Dell'Osso, "Dynamic properties of the human vestibulo-ocular reflex during head rotations in roll," *Vis. Res.*, vol. 35, no. 5, pp. 679–689, 1995.
[55] E. L. Keller, "Oculomotor neuron behavior," in *Models of oculomotor behavior and control*, B. L. Zuber, Ed. Boca Raton, FL: CRC Press, 1981, pp. 1–19.
[56] A. F. Fuchs, C. A. Scudder, and C. R. S. Kaneko, "Discharge patterns and recruitment order of identified motoneurons and internuclear neurons in the monkey abducens nucleus," *J. Neurophysiol.*, vol. 60, no. 6, pp. 1874–1895, 1988.
[57] J. S. Stahl and J. I. Simpson, "Dynamics of abducens nucleus neurons in the awake rabbit," *J. Neurophysiol.*, vol. 73, pp. 1383–1395, 1995.
[58] N. F. Lepora, J. Porrill, C. H. Yeo, C. Evinger, and P. Dean, "Recruitment in retractor bulbi muscle during eyeblink conditioning: EMG analysis and common-drive model," *J. Neurophysiol.*, vol. 102, no. 4, pp. 2498–2513, Doi: 10.1152/jn.00204.2009.
[59] G. Lennerstrand, "Mechanical studies on the retractor bulbi muscle and its motor units in the cat," *J. Physiol.*, vol. 236, pp. 43–55, 1974.
[60] A. Fuchs, C. Kaneko, and C. Scudder, "Brainstem control of saccadic eye movements," *Annu. Rev. Neurosci.*, vol. 8, pp. 307–337, 1985.
[61] C. Scudder and A. Fuchs, "Physiological and behavioral identification of vestibular nucleus neurons mediating the horizontal vestibuloocular reflex in trained monkeys," *J. Neurophysiol.*, vol. 68, pp. 244–264, 1992.
[62] C. A. Scudder, C. R. S. Kaneko, and A. F. Fuchs, "The brainstem burst generator for saccadic eye movements: A modern synthesis," *Exp. Brain Res.*, vol. 142, pp. 439–462, 2002.
[63] T. Hazel, S. Sklavos, and P. Dean, "Estimation of premotor synaptic drives to simulated abducens motoneurons for control of eye position," *Exp. Brain Res.*, vol. 146, no. 2, pp. 184–196, 2002.
[64] L. Ling, A. F. Fuchs, C. Siebold, and P. Dean, "Effects of initial eye position on saccade related behavior of abducens nucleus neurons in the primate," *J. Neurophysiol.*, vol. 98, pp. 3581–3599, 2007.
[65] D. Bers, "Cardiac excitation-contraction coupling," *Nature*, vol. 415, no. 10, pp. 198–205, Jan. 2002.
[66] F. Zajac, "Muscle and tendon: Properties, models, scaling and application to biomechanics and motor control," *Crit. Rev. Biomed. Eng.*, vol. 17, no. 4, pp. 359–411, 1989.
[67] G. Zahalak, "An overview of muscle modelling," in *Neural Prostheses: Replacing Motor Function After Injury or Disease*, R. Stein, P. Peckam, and D. Popovic, Eds. New York: Oxford Univ. Press, 1992, pp. 17–57.
[68] W. Durfee, "Model identification in neural prosthesis systems," in *Neural Prostheses: Replacing Motor Function after Injury or Disease*, R. Stein, P. Peckam, and D. Popovic, Eds. New York: Oxford Univ. Press, 1992, pp. 58–87.
[69] H. Gollee, D. J. Murray-Smith, and J. C. Jarvis, "A nonlinear approach to modeling of electrically stimulated skeletal muscle," *IEEE Trans. Biomed. Eng.*, vol. 48, no. 4, pp. 406–415, Apr. 2001.
[70] F. Previdi, "Identification of black-box nonlinear models for lower limb movement control using functional electrical stimulation," *Control Eng. Pract.*, vol. 10, pp. 91–99, 2002.
[71] P. Dean, "Motor unit recruitment in a distributed model of extraocular muscle," *J. Neurophysiol.*, vol. 76, no. 2, pp. 727–742, 1996.
[72] M. S. Shall, D. M. Dimitrova, and S. J. Goldberg, "Extraocular motor unit and whole-muscle contractile properties in the squirrel monkey. Summation of forces and fiber morphology," *Exp. Brain Res.*, vol. 151, no. 3, pp. 338–345, 2003.
[73] J.-J. Slotine and W. Li, *Applied Nonlinear Control*. Englewood Cliffs, NJ: Prentice-Hall, 1991.
[74] T. Nichols and J. Houk, "Improvement in linearity and regulation of stiffness that results from actions of stretch reflex," *J. Neurophysiol.*, vol. 39, pp. 119–142, 1976.
[75] F. A. Mussa-Ivaldi, S. F. Giszter, and E. Bizzi, "Linear combinations of primitives in vertebrate motor control," *Proc. Natl. Acad. Sci. U.S.A.*, vol. 91, no. 16, pp. 7534–7538, 1994.

Sean R. Anderson was born in Reading, U.K. He received the M.Eng. degree in control systems engineering from the Department of Automatic Control and Systems Engineering, University of Sheffield, Sheffield, U.K., in 2001, and the Ph.D. degree from the Department of Chemical and Process Engineering, University of Sheffield, in 2005.

He is currently a Research Associate at the Centre for Signal Processing in Neuroimaging and Systems Neuroscience and Department of Psychology, University of Sheffield, where he has been engaged in the research on the central nervous system, using systems engineering techniques to investigate biological adaptive control. His research interests include identification of continuous- and discrete-time dynamic systems, nonlinear systems modeling, oculomotor plant dynamics, computation and function of the cerebellum, and the study of adaptive and optimal control in biological systems.

Nathan F. Lepora received the B.A. degree in mathematics and the Ph.D. degree in theoretical physics from the University of Cambridge, Cambridge, U.K.

He was a Research Fellow with Kings College, University of Cambridge, Cambridge, U.K., for four years. He then joined the Department of Psychology, University of Sheffield, Sheffield, U.K., where he was engaged in research on the cerebellum and motor control with P. Dean and J. Porrill. He is currently a Research Associate with the Adaptive Behaviour Research Group at the Centre for Signal Processing in Neuroimaging and Systems Neuroscience and Department of Psychology, University of Sheffield, where his research has been focused on various topics related to basal ganglia function.

John Porrill received the Ph.D. degree from the University of Cambridge, Cambridge, U.K., while working with J. Stewart on topics in classical general relativity.

He is currently at the Centre for Signal Processing in Neuroimaging and Systems Neuroscience and Department of Psychology, University of Sheffield, Sheffield, U.K., where he has been involved in the research on human and computer vision with J. Mayhew and J. Frisby. His research interests include the psychophysics of human stereo vision, video tracking of eye movements, building the EyeLab open source model of the extraocular muscle system, and computational models of the role of the cerebellum in the control of eye movements.

Paul Dean received the M.A. degree in physiology with psychology from the University of Cambridge, Cambridge, U.K., and the D.Phil. degree from the University of Oxford, Oxford, U.K.

He is currently a Professor in the Department of Psychology and a Member of the Centre for Signal Processing in Neuroimaging and Systems Neuroscience, University of Sheffield, Sheffield, U.K. His research interests include producing computational models of neural systems that are based on both biological data and current developments in control engineering, signal processing, and robotics. These models are intended to serve as a vehicle for two-way communication between biological and physical sciences, allowing roboticists to use new discoveries in biology, and biologists to interpret their findings in the light of current developments in signal processing.